Bilateral Comparison Confirms NIM's and NIST's Gas Flow Capabilities

Chunhui Li
National Institute of Metrology (NIM), P. R. China
Tel: 086-010-64525122, Fax: 86-10-64525126, Email: lich@nim.ac.cn

Aaron Johnson
National Institute of Standards and Technology (NIST), Gaithersburg, U. S. A
Tel: 001-301-975-5954, Email: aaron.johnson@nist.gov

Abstract: A bilateral comparison of the gas flow standards of the National Institute of Metrology (NIM) in China and the National Institute of Standards and Technology (NIST) in the USA was conducted from June 2008 to October 2009. Two critical flow venturis (CFVs) with nominal throat diameters of 10 mm and 20 mm, respectively, were selected as transfer standards. The CFVs were calibrated on NIM's 20 m^3 *PVTt* system and then on NIST's 26 m^3 *PVTt* system. The results demonstrate the equivalence between NIM's and NIST's gas flow measurement capabilities for flows ranging from 1000 liters per minute to 4000 liters per minute at reference conditions of 101.325 kPa and 293.15 K. The experimental data agreed with existing theoretical models within 0.07 %. All the data agree with the ISO 9300 empirical equation within its 0.3 % expanded uncertainty limit.

Keyword: critical flow venturi (CFV), sonic nozzle, *PVTt* facility, NIM and NIST bilateral flow comparison

1. Introduction

National Metrology Institutes (NMIs) periodically compare their primary standards to validate their claimed measurement capabilities. For gas flow, the critical flow venturi (CFV) or sonic nozzle is among the world's best transfer standard and has been used successfully for numerous inter-comparisons between NMIs as well as between secondary flow calibration laboratories. The three main advantages of CFVs over other gas flowmeters are their excellent long-term reproducibility [1], well established flow models that accurately predict CFV performance, and straightforward application. In this work two CFVs with throat diameters of 10 mm and 20 mm are used to compare the primary standards of the National Institute of Metrology (NIM) in China with those of National Institute of Standards and Technology (NIST) in the U.S. The NIST primary standard is a 26 m^3 blow down type *PVTt* system with an expanded uncertainty in mass flow of 0.09 % (k = 2) [2] while the NIM primary standard is a 20 m^3 suction type *PVTt* system with an expanded uncertainty in mass flow of 0.05 % (k = 2). The CFV mass flows measured by the respective *PVTt* systems are used to calculate the discharge coefficient, the parameter compared in this bilateral. The comparison results are in good agreement, differing by less than 0.017 % for the 10 mm CFV and less than 0.11 % for the 20 mm CFV. These results validate the claimed measurement capabilities of both NMIs as demonstrated by the degree of equivalence (*i.e.*, E_n[a] numbers) being less than unity in Fig. 1.

[a] The degree of equivalence is the difference between the measured C_d values of NIM and NIST divided by the total expanded uncertainty as shown in Eq. (10).

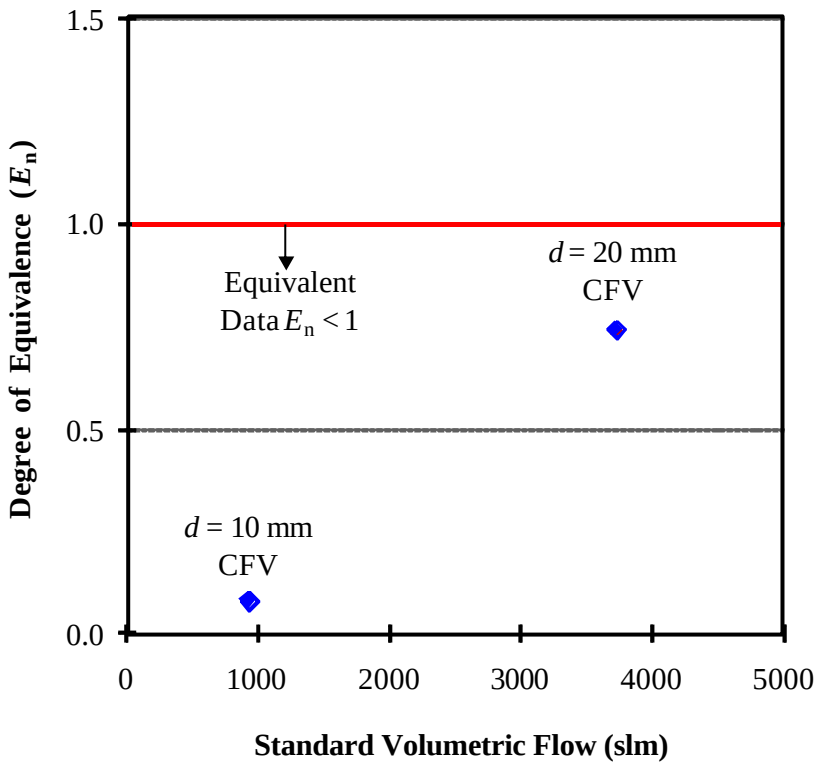

Fig. 1 Degree of Equivalence for 2 CFVs used in bilateral comparison between NIM and NIST[a].(The reference conditions for the standard volumetric flow are 101.325 kPa and 293.15 K.)

The NIST *blow down type PVTt* system calibrates CFVs in dry air at pressures ranging from 170 kPa to 800 kPa. In contrast, the NIM *suction type PVTt* system calibrates CFVs using humid air at atmospheric pressure. The mismatch in the upstream CFV pressures between the NIST and NIM *PVTt* systems corresponds to a gap in the flow range (or Reynolds numbers) over which the CFVs are compared. For example, NIST calibrated the 10 mm CFV over a Reynolds number range extending from 2.16×10^5 to 1.01×10^6 while NIM calibrated the same CFV at a Reynolds number of 1.3×10^5. The gap in flow conditions is accounted for by extrapolating the NIST results to lower Reynolds numbers. In particular, the measured discharge coefficients are extrapolated as a linear function of the inverse square-root of the Reynolds number. This functional dependence on the Reynolds number is based on well established laminar CFV theory [3] and has been experimentally verified by numerous researchers [4, 5]. Moreover, similar extrapolation methods have been used successfully in other comparisons where CFVs were used as transfer standards [6].

2. CFV Operating Principle

Critical flow venturis operate at downstream-to-upstream pressure ratios sufficient to establish sonic velocities at the throat cross section. The maximum pressure ratio that establishes sonic throat conditions is called the critical back pressure ratio, and CFVs must be operated at or below this ratio. Once sonic throat conditions are obtained, the CFV mass flow depends only on the upstream stagnation conditions. Decreasing the downstream pressure has no effect on the mass flow. Physically, pressure waves caused by varying the downstream pressure cannot propagate upstream of the sonic conditions at the CFV throat. If the CFV flow process is assumed to be 1) one-dimensional, and 2) isentropic, the ideal mass flow is given by

$$q_{mi} = \frac{p d^2 P_0 C_* \sqrt{M}}{4\sqrt{R_u T_0}} \quad (1)$$

where d is the CFV throat diameter, C_* is the critical flow function which corrects for the virial coefficients of the gas, P_0 is the upstream stagnation pressure, T_0 is stagnation temperature, R_u is the universal gas constant, and M is the molar mass of the gas.

The assumptions of one-dimensional, isentropic flow are never perfectly realized. First, momentum losses and viscous dissipation in the boundary layer violate the isentropic assumption. Second, in the core flow outside the boundary layer, the locus where the flow becomes sonic is not planar; instead it is a function of the shape of the CFV throat. Therefore, the one-dimensional isentropic mass flow model is corrected by the discharge coefficient

$$C_d = \frac{q_{mr}}{q_{mi}} = \frac{4 q_{mr} \sqrt{R_u T_0}}{p d^2 P_0 C_* \sqrt{M}} \quad (2)$$

a dimensionless ratio of the actual mass flow (q_{mr}) to the ideal mass flow (q_{mi}) that plays a central role in CFV flow calibrations.

For a given CFV geometry and gas type, C_d is a function of the Reynolds number alone

$$Re'_d = \frac{4 q_{mr}}{p d \mu_0} \quad (3)$$

where μ_0 is dynamic viscosity evaluated at P_0 and T_0. Since the Reynolds number definition in Eq. (3) depends on mass flow (which is typically the unknown parameter that is being measured), the theoretical Reynolds number

$$Re_d = \frac{4 q_{mi}}{p d \mu_0} \quad (4)$$

which is based on the ideal mass flow, is often a more convenient choice. The two Reynolds number definitions are related by the discharge coefficient, $Re_d = Re'_d / C_d$. The C_d verses Re_d plot is called the CFV calibration curve. In practice, three methods are used to determine the calibration curve. They are 1) calibrating the CFV against a reference standard (*e.g.*, a primary standard, another flowmeter); 2) using empirical C_d values provided in paper standards such as the ISO 9300 document [7]; and 3) using theoretical C_d values obtained from analytical [8-11] or numerical solutions of the Navier-Stokes Equations. The latter two approaches require accurate throat diameter measurements to convert from C_d to mass flow when the CFV is used in application. The second method also requires that the CFV geometry adhere to ISO 9300 specifications, and the third method requires a measurement of the curvature parameter at the CFV throat, $O^* = d/2r_c^*$ where r_c^* is the throat radius of curvature.

The empirical C_d values given in the ISO 9300 document, as well as theoretically calculated C_d values, are compared to the *PVTt* results of NIM and NIST. The ISO 9300 calibration curve

$$C_{d,ISO} = 0.9959 - \frac{2.720}{\sqrt{Re'_d}} \quad (5)$$

expresses the discharge coefficient as a function of the actual Reynolds number. The fit has an expanded uncertainty of 0.3 % (k = 2) and is valid over a Reynolds number range from 2.1×10^4 to 3.2×10^7. The theoretical calibration curve uses a composite model that accounts for both viscous effects due to the boundary layer along the CFV wall (*i.e.*, $C_{\mathrm{d,BL}}$) and for the axisymmetric density and velocity profile in the inviscid core outside the boundary layer (*i.e.*, $C_{\mathrm{d,2D}}$)

$$C_{\mathrm{d,theory}} = C_{\mathrm{d,BL}}\, C_{\mathrm{d,2D}}$$

or

$$C_{\mathrm{d,theory}} = \left(1 - a_1 O^{*-\mathrm{m}}\, Re_{\mathrm{d}}^{\ -\mathrm{n}} + a_2 O^{*-2\mathrm{m}}\, Re_{\mathrm{d}}^{\ -2\mathrm{n}}\right)\left(1 - \frac{b_2}{\Lambda^2} + \frac{b_3}{\Lambda^3} + \frac{b_4}{\Lambda^4}\right) \tag{6}$$

where $\Lambda = 1 + 1/O^*$ is the expansion parameter and the other coefficients and exponents are specified in Tables 1 and 2. We point out that for ISO 9300 shaped CFVs with Reynolds numbers above 100 000, the term ($a_2 O^{*-2\mathrm{m}}\, Re_{\mathrm{d}}^{\ -2\mathrm{n}}$) contributes less than 0.004 % and can be neglected. Consequently, the discharge coefficient scales linearly with $Re_{\mathrm{d}}^{-1/2}$ in the laminar flow regime, which is the basis of the extrapolation method discussed in the introduction. Transition from laminar to turbulent flow occurs at Reynolds number of approximately 10^6 provided the CFV wall is smooth with no geometric defects near the throat. Transition to turbulent flow can occur at smaller Reynolds numbers if the boundary layer is perturbed by geometric defects near the throat or by excessive wall roughness.

Table 1. Coefficients and exponents for calculating $C_{\mathrm{d,BL}}$ in Eq. (6)

Boundary Layer Models	**Flow Type**	**Exponents**		**Coefficients**	
		m	n	a_1	a_2
Geropp[10]	Laminar $Re_{\mathrm{d}} < 10^6$	1/4	1/2	$2\left[\frac{(g-7)\sqrt{6}+18}{3}\right]\left(\frac{g+1}{2}\right)^{-3/4}$	$\left[\frac{(g-7)\sqrt{6}+18}{3}\right]^2\left(\frac{g+1}{2}\right)^{-3/2}$
Stratford[11]	Turbulent $Re_{\mathrm{d}} = 10^6$	2/5	1/5	$\left(\frac{21}{400}\right)\left(\frac{1}{2}\right)^{2/5}\left(\frac{m^*}{m_0}\right)^{1/5}$	0

Table 2. Coefficients for calculating $C_{\mathrm{d,2D}}$ in Eq. (6)

Inviscid Axisymmetric Model	**Expansion parameter, Λ**	**Series Expansion Coefficients**		
		b_2	b_3	b_4
Kliegel and Levine [9]	$\Lambda \equiv 1 + \frac{1}{O^*}$	$\frac{g+1}{96}$	$\frac{(g+1)(8g-27)}{2{,}304}$	$\frac{(g+1)(754g^2 - 757g + 3{,}633)}{552{,}960}$

In the remainder of this document we describe NIM's 20 m^3 *PVTt* system and NIST's 26 m^3 *PVTt* system. These *PVTt* systems are used to calibrate the two transfer standards (*i.e.*, the 10 mm and 20 mm CFVs). The measured C_{d} values are compared using the extrapolation method. The experimentally measured calibration curves are also compared to the empirical $C_{\mathrm{d,ISO}}$ values

given in the ISO 9300 document, and the theoretical $C_{d,theory}$ values obtained from a composite (*i.e.*, boundary layer and inviscid core) CFV model. Dimensional measurements of the CFV throat diameters and curvature parameters made at NIST and NIM are presented.

3. Description of NIM's and NIST's Flow Calibration Facilities

3.1. NIM's 20 m^3 *PVTt* Primary Flow Standard

Figure 2 shows a schematic of NIM's 20 m^3 suction type *PVTt* primary flow standard. Temperature, pressure, and relative humidity instrumentation are used in conjunction with an equation of state to determine the density in the collection tank before and after filling. The working fluid is humid air at atmospheric pressure. The *PVTt* system works by first evacuating the 20 m^3 collection vessel to a pressure of 500 Pa using a vacuum pump. The density of the air remaining in the tank is determined. Subsequently, the tank inlet valve is opened while simultaneously starting the timer. During the filling process, ambient air flows through the CFV into the collection tank. When the collection tank is filled to approximately 50 kPa, the tank inlet valve is closed and simultaneously, the timer is stopped. Once thermal equilibrium is established in the collection tank, the final air density is calculated. The difference between the final and initial air density is multiplied by the collection tank volume to determine the mass change in the collection tank attributed to the filling process. The time-averaged mass flow through the CFV is the mass change in the collection tank divided by the collection time interval.

The ideal CFV flow is calculated using Eq. (1) with corrections made for relative humidity. The CFV discharge coefficient is determined by dividing the mass flow measured using the *PVTt* by the ideal CFV mass flow given in Eq. (2). Since the CFV upstream stagnation pressure is limited to atmospheric conditions, the C_d can only be measured at a single Reynolds number. For the 10 mm CFV the Reynolds number is 1.3×10^5 while for the 20 mm CFV the Reynolds number is 2.6×10^5. The expanded uncertainty for mass flow using NIM's 20 m^3 *PVTt* is 0.05 % (k = 2) and the expanded uncertainty for the discharge coefficient ranges from 0.10 % to 0.20 % (k = 2) depending on the reproducibility of repeated measurements.

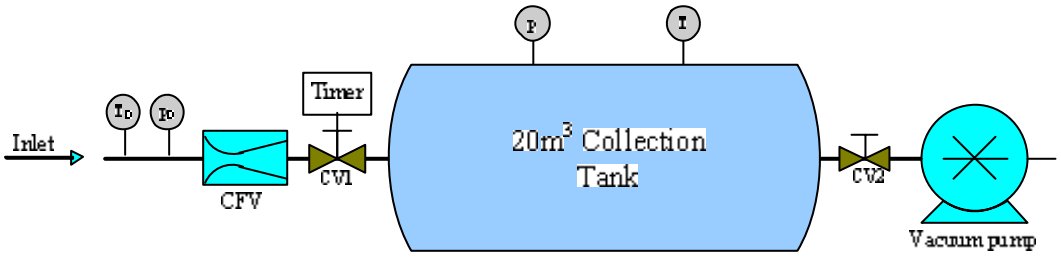

Fig. 2 NIM's 20 m^3 PVTt primary flow standard

3.2. NIST's 26 m^3 *PVTt* Primary Flow Standard

Figure 3 shows a schematic of NIST's 26 m^3 blow down *PVTt* primary flow standard. This *PVTt* standard determines the CFV mass flow using a timed-collection technique whereby a steady source of flow accumulates into an initially evacuated collection vessel for a measured time interval. The mass flow is the product of the collection tank volume and the density change in the collection tank divided by the measured time interval. The specific details on the operation and uncertainty analysis of the 26 m^3 *PVTt* are found in other publications [2, 12]. The flow source is dry air pressurized between 170 kPa and 800 kPa at ambient temperatures. For this pressure

range the Reynolds number for the 10 mm CFV varies from 2.16×10^5 to 1.01×10^6 while the Reynolds number for the 20 mm CFV varies from 4.3×10^5 to 2×10^6. For both CFVs the laminar flow extrapolation technique is used to close the gap between the different Reynolds number ranges measured at NIST and NIM. The expanded uncertainty of NIST's mass flow measurements is 0.09 % (k = 2) while the expanded uncertainty of the discharge coefficient is 0.10 % (k = 2).

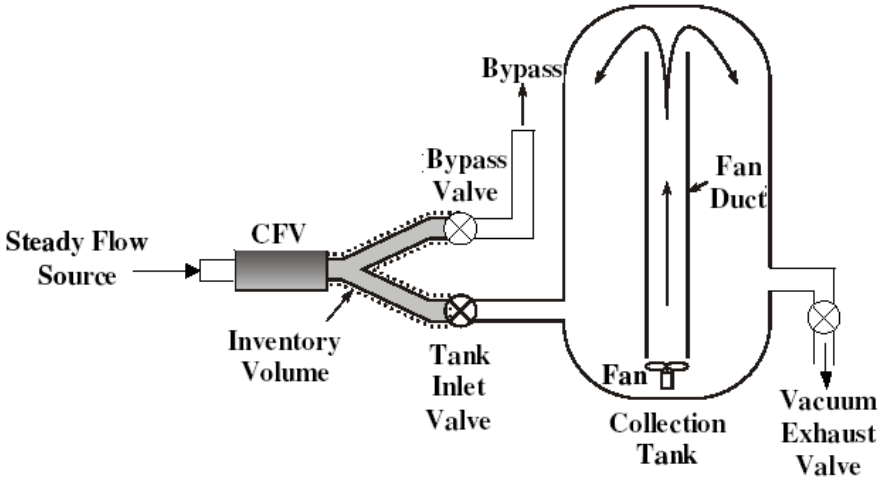

Fig. 3 NIST 26 m^3 PVTt primary flow standard

4. Dimensional Measurements of the CFV Geometry

Accurate measurements of the CFV throat diameter (d) and throat curvature parameter (O^*) are needed to assess how well the measured NIM and NIST C_d values agree with $C_{d,theory}$ given in Eq. (6). In addition, dimensional measurements are needed to verify that the curvature of the convergent section adheres to ISO 9300 specifications so that the $C_{d,ISO}$ given in Eq. (5) can be reliably compared to the measured C_d values. NIM and NIST both measured the throat diameter and curvature parameter of the two CFVs. However, NIM measured the *global* curvature parameter (O) from the CFV inlet to the throat to validate that the CFV shape followed the ISO 9300 protocol. In contrast, NIST measured the *local* curvature parameter at the CFV throat (O^*) to calculate $C_{d,theory}$.

4.1. NIM's Dimensional CFV Measurements

A Leitz 3D[b] coordinate measurement machine (CMM) was used to measure the geometry of both the 10 mm and 20 mm CFVs. The standard (k = 1) uncertainty of length measurements made using this CMM is $(0.6 + l/600)$ µm where the length dimension of l is in millimeters. The expanded uncertainty of the throat diameter measurement is estimated to be 5 µm (k = 2).

The CFV throat diameter was determined using a least squares linear regression analysis. Measurements of the average diameter are made at 20 µm intervals in the axial direction, beginning upstream of the throat and continuing to the downstream side. Least squares regression is used to find the best-fit curve through these average diameter measurements. The diameter at

[b] Certain commercial equipment, instruments, or materials are identified in this paper to foster understanding. Such identification does not imply recommendation or endorsement by the National Institute of Standards and Technology, nor does it imply that the materials or equipment identified are necessarily the best available for the purpose.

the zero slope location of this fit is taken to be the throat diameter. The average diameter at each cross section is determined by fitting the best-fit circle to between 40 and 50 CMM measurements.

The average curvature of the CFV convergent section was measured to ensure that it was consistent with ISO 9300 specifications, (*i.e.*, $0.2273 = O_{\mathrm{ISO}} = 0.2778$). The radius of curvature was measured from the CFV entrance to the throat section at 80 to 100 cross sectional planes. In each plane, 8 CMM measurements were taken spaced 45 degrees apart. Each of the eight angles corresponds to a curve along the CFV wall that spans from the entrance to the throat. The radius of curvature is taken to be the average radius of curvature these 8 curves, and the curvature parameter is calculated as the throat diameter divided by twice the radius of curvature.

4.2. NIST's Dimensional CFV Measurements

The NIST Moore M48 3D[b] coordinate measurement machine was used to determine the CFV throat diameter and throat curvature parameter. The expanded uncertainty of the throat diameter measurement is estimated to be 1 µm ($k = 2$). The throat diameters of the two CFVs are determined by traversing the probe of the Moore M48 along the nozzle wall through the throat region. At each cross section, the probe makes twelve radial measurements spaced 30° apart. The average of these twelve measurements is taken to be the average radius of the best fit circle. The CFV profile is estimated using either a fifth or sixth degree polynomial that expresses the average radius as a function of axial position. The axial position of the throat is determined by setting the derivative of the polynomial equal to zero. The throat diameter (d) equals twice the value of the polynomial evaluated at the axial throat location, and the throat curvature ($1/r_{\mathrm{c}}^{*}$) equals the second derivative of the polynomial evaluated at the throat location. The throat curvature parameter is calculated by multiplying the throat diameter by the curvature and dividing by two, ($O^{*} = d/2r_{\mathrm{c}}^{*}$).

4.3. Comparison of NIM's and NIST's Dimensional Measurements

The throat diameters measured by NIM and NIST agreed to within the uncertainties specified by the two NMIs. For the $d = 10$ mm CFV the difference between NIM and NIST is 1.89 µm or -0.0189 %, and for the $d = 20$ mm CFV the difference is 0.23 µm or 0.001 %. The differences between the measured values of the curvature parameter are substantially larger as expected, being 5.5 % for the 10 mm CFV, and 1.7 % for the 20 mm CFV. However, the influence of the curvature parameter on CFV performance is less significant than the throat diameter. Because the discharge coefficient varies as d^{-2} as shown in Eq. (2), a 0.1 % error in the throat diameter results in a 0.2 % error in C_{d}. On the other hand, a 5.5 % error in the curvature parameter of an ISO 9300 shaped CFV changes the C_{d} by less than 0.01 % (according to theory). The dimensional measurements of NIM and NIST are summarized in Table 1.

Table 1. Comparison of dimensional measurements of the CFV throat diameter and curvature parameter of NIM and NIST

Nom. Dia.	**NIM Measurements**			**NIST Measurements**			**% Difference between NIM and NIST Measurements**	
d_{nom} [mm]	d [mm]	r_c [mm]	O [ ]	d [mm]	r_c^* [mm]	O^* [ ]	$d_{NIM} - d_{NIST}$ [%]	$O_{NIM} - O^*_{NIST}$ [%]
10	10.0006	19.797	0.2526	10.0025	18.719	0.2672	-0.019	-5.5
20	19.9907	39.738	0.2515	19.9910	40.432	0.2472	-0.0015	1.7

4.4. Circularity of the CFV Cross Sections

Figure 3 shows cross sectional views of the d = 10 mm and d = 20 mm CFVs at different axial distances upstream and downstream of the throat location. At each axial location 12 radii are measured 30 degrees apart. The difference between each of the 12 radial measurements is subtracted by the average radius (*i.e.*, the arithmetic average of the 12 radial measurements) is defined as the *deviation from circularity* and plotted in the figure in millimeters. The 10 mm CFV shows 12 deviation plots starting 1.5 mm upstream of the throat and extending 1 mm beyond the throat. Likewise, the 20 mm CFV shows 12 deviation plots starting 2 mm upstream of the throat to 1 mm downstream of the throat section. For comparison purposes, both plots have the same scaling, varying from -0.02 mm to 0.005 mm. The d = 10 mm CFV has a defect at approximately 270 degrees that results in a deviation from circularity of 0.013 mm or approximately 0.1 % of the throat diameter. In contrast, the d = 20 mm CFV does not deviate from circularity by more than 0.001 mm.

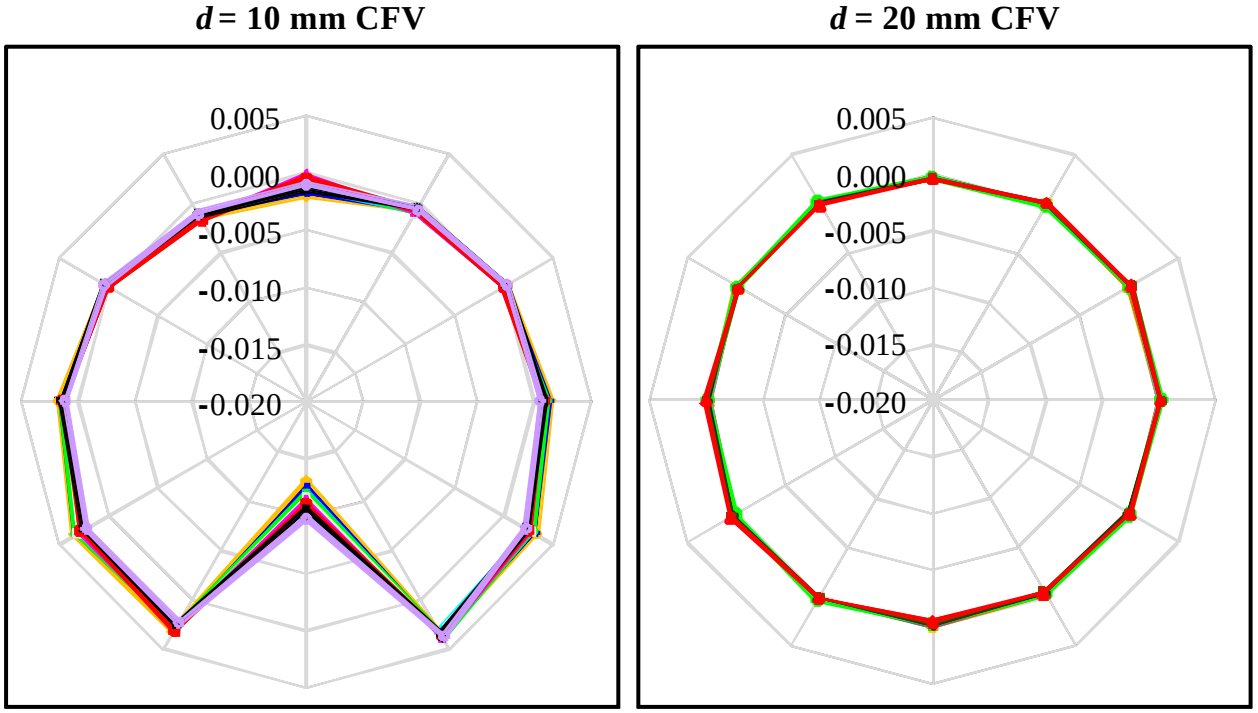

Fig. 3. Cross sectional views showing the deviation from circularity (in millimeters) of the d = 10 mm and d = 20 mm CFVs in the vicinity of the throat.

5. Experimental Results and Analysis

5.1. NIM's Calibration Results

The 10 mm and 20 mm CFVs were calibrated on NIM's 20 m^3 *PVTt* standard during a 5 month period from June 8, 2008 to October 19, 2008. The calibration results are shown in Tables 2 and 3 respectively.

Table 2. NIM's calibration results for the 10 mm CFV using the 20 m^3 PVTt system

P_0 [kPa]	T_0 [K]	RH [%]	C_* [ ]	No. of Repeat Points **[ ]**	Stdev. of Repeated C_d Meas. **[%]**	Re_d **[ ]**	$1/\sqrt{Re_d}$ **[ ]**	C_d **[ ]**
101.23	294.19	61	0.68513	3	0.04	1.31×10^5	0.002765	0.9882
100.80	294.02	71	0.68513	6	0.04	1.31×10^5	0.002768	0.9877
99.46	297.17	77	0.68511	6	0.04	1.28×10^5	0.002799	0.9894
100.69	295.83	93	0.68512	3	0.03	1.30×10^5	0.002773	0.9881
					Average	**1.30×10^5**	**0.002776**	**0.98835**

Table 3. NIM's calibration results for the 20 mm CFV using the 20 m^3 PVTt system

P_0 [kPa]	T_0 [K]	RH [%]	C_* [ ]	No. of Repeat Points [ ]	Stdev. of Repeated C_d Meas. [%]	Re_d [ ]	$1/\sqrt{Re_d}$ [ ]	C_d [ ]
102.48	293.50	20	0.68514	3	0.04	2.64×10^5	0.001945	0.9910
102.12	294.75	43	0.68513	3	0.03	2.63×10^5	0.001949	0.9911
100.57	297.56	48	0.68511	6	0.02	2.57×10^5	0.001973	0.9914
100.18	296.70	54	0.68511	6	0.04	2.56×10^5	0.001975	0.9914
100.45	298.96	73	0.68510	6	0.03	2.57×10^5	0.001974	0.9917
					Average	**2.59×10^5**	**0.001963**	**0.99132**

5.2. NIST's Calibration Results

The 10 mm and 20 mm CFV transfer standards were calibrated using NIST's 26 m^3 *PVTt* primary flow standard. The calibrations began on September 4, 2009 and finished on September 25, 2009. The results of these calibrations are shown in Tables 4 and 5, respectively.

Table 4. NIST's calibration results for the 10 mm CFV using the 26 m^3 PVTt system

P_0 [kPa]	T_0 [K]	C_* [ ]	Re_d [ ]	$1/\sqrt{Re_d}$ [ ]	C_d [ ]	No. of Repeat Points [ ]	Stdev. of Repeat C_d Meas. [%, k = 1]	Expanded Unc. $U_{C_d} = k u_{C_d}$ [%, k = 2]
170.37	298.13	0.68528	2.16×10^5	0.002153	0.99077	14	0.005	0.10
180.37	298.05	0.68531	2.29×10^5	0.002092	0.99131	3	0.002	0.10
190.37	297.80	0.68534	2.41×10^5	0.002035	0.99193	4	0.001	0.10
200.37	298.28	0.68537	2.54×10^5	0.001986	0.99241	23	0.002	0.10
227.37	298.66	0.68544	2.87×10^5	0.001866	0.99287	10	0.003	0.10
319.36	298.77	0.68568	4.03×10^5	0.001575	0.99386	8	0.007	0.10
480.36	298.97	0.68610	6.05×10^5	0.001285	0.99479	7	0.003	0.10
650.37	299.44	0.68654	8.17×10^5	0.001106	0.99525	8	0.004	0.10
800.37	299.26	0.68694	1.01×10^6	0.0009970	0.99507	9	0.002	0.10

Table 5. NIST's calibration results for 20 mm CFV using the 26 m^3 PVTt system

P_0 [kPa]	T_0 [K]	C_* [ ]	Re_d [ ]	$1/\sqrt{Re_d}$ [ ]	C_d [ ]	No. of Repeat Points [ ]	Stdev. of Repeat C_d Meas. [%, k = 1]	Expanded Unc. $U_{C_d} = k u_{C_d}$ [%, k = 2]
170.38	298.35	0.68528	4.31×10^5	0.0015234	0.99376	8	0.002	0.10
210.37	298.58	0.68539	5.31×10^5	0.0013717	0.99431	3	0.005	0.10
250.37	298.30	0.68550	6.33×10^5	0.0012568	0.99461	5	0.002	0.10
300.37	298.35	0.68563	7.59×10^5	0.0011477	0.99499	7	0.003	0.10
350.36	297.41	0.68579	8.89×10^5	0.0010606	0.99525	8	0.003	0.10
400.36	297.74	0.68591	1.01×10^6	0.0009930	0.99547	5	0.006	0.10
450.36	297.92	0.68604	1.14×10^6	0.0009367	0.99552	5	0.003	0.10
500.37	298.01	0.68617	1.27×10^6	0.0008889	0.99515	7	0.006	0.10
600.37	298.29	0.68643	1.52×10^6	0.0008122	0.99422	7	0.003	0.10
700.38	298.74	0.68669	1.76×10^6	0.0007529	0.99425	5	0.006	0.10
800.38	297.88	0.68698	2.02×10^6	0.0007031	0.99425	7	0.005	0.10

5.3. Uncertainty Analysis

The combined standard uncertainty of the discharge coefficient is calculated as the root-sum-square of the products of the standard uncertainties of each contributing factor in Eq. (2) multiplied by their sensitivity coefficients[13],

$$u_{C_\mathrm{d}} = \sqrt{u_{q_\mathrm{mr}}^2 + u_{P_0}^2 + \frac{1}{4}u_{T_0}^2 + u_{C_*}^2 + \frac{1}{4}u_M^2 + \frac{1}{4}u_{R_\mathrm{u}}^2 + 4u_d^2 + u_\mathrm{reprd}^2}\ . \tag{7}$$

Here we also include the uncertainty attributed to the reproducibility (u_reprd) taken to be equal to the standard deviation of repeated measurements. In this comparison, identical values of R_u and d are used by both NIM and NIST so that the standard uncertainties u_{R_u} and u_d in Eq. (7) are taken to be zero.[c] The fluid properties M and C_* used by NIM and NIST differ only due to the mole fraction of water vapor (x_v) in the air. NIM's *PVTt* system used humid air with x_v varying from 0.0054 to 0.0225 while NIST dried the air to maintain x_v less than 0.00035. The relationships between the molar mass (M_humid) and critical flow function ($C_{*,\mathrm{humid}}$) of humid air relative to the molar mass (M_dry) and critical flow function ($C_{*,\mathrm{dry}}$) of dry air are

$$\frac{M_\mathrm{humid}}{M_\mathrm{dry}} = 1 - x_v\left(1 - \frac{M_{\mathrm{H_2O}}}{M_\mathrm{dry}}\right) \tag{8a}$$

and

$$\frac{C_{*,\mathrm{humid}}}{C_{*,\mathrm{dry}}} = f(x_v)\,, \tag{8b}$$

where $M_{\mathrm{H_2O}}$ is the molar mass of water, and the functional forms for $f(x_v)$ are given by Aschenbrenner [14] and by Britton *et. al.* [15]. In this comparison, NIM and NIST use nearly identical values for M_dry and $C_{*,\mathrm{dry}}$ so that only the water vapor content contributes to the uncertainty in the discharge coefficient, and Eq. (7) can be conveniently expressed as

$$u_{C_\mathrm{d}} = \sqrt{u_{q_\mathrm{mr}}^2 + u_{P_0}^2 + \frac{1}{4}u_{T_0}^2 + (S_{x_v}u_{x_v})^2 + u_\mathrm{reprd}^2}\ , \tag{9}$$

where u_{x_v} is the relative standard uncertainty of the mass fraction of water vapor multiplied by its sensitivity coefficient. For the NIM CFV calibrations the nominal value of the sensitivity coefficient is $S_{x_v} \approx$ -0.007, while at NIST the sensitivity coefficient is taken to be zero, $S_{x_v} = 0$, since the effect of x_v = 0.00035 on C_d is negligible.

The CFV calibrations were repeated many times over a period of 5 months at NIM and over a 3 week period at NIST. The repeated measurements were used to assess the reproducibility of the CFV calibrations. The standard uncertainty components, combined uncertainties, and expanded uncertainties for both the 10 mm and 20 mm CFVs are itemized in Tables 6 and 7 respectively.

[c] While the uncertainties of R_u and d can be taken to be zero for the comparison between NIM and NIST, these uncertainties should be included when compared to the theoretical model and the ISO 9300 empirical curve fit.

Table 6. Relative uncertainty components for the calibration of the 10 mm CFV

Standard Uncertainty Sources	NIM [%, k = 1]	NIST [%, k = 1]
PVTt mass flow, $u_{q_{mr}}$	0.025	0.045
Stagnation temperature, u_{T_0}	0.020	0.03
Stagnation pressure, u_{p_0}	0.008	0.02
Mole fraction of water vapor, u_{x_v}	2.89	0
Reproducibility, u_{reprd}	0.082	< 0.01
Std. Combined Uncertainty Eq. (9), u_{C_d}	**0.09**	**0.05**
Expanded Uncertainty $U_{C_d} = k u_{C_d}$	[%, k = 2] **0.18**	[%, k = 2] **0.10**

Table 7. Relative uncertainty components for the calibration of the 20 mm CFV

Standard Uncertainty Sources	NIM [%, k = 1]	NIST [%, k = 1]
PVTt mass flow, $u_{q_{mr}}$	0.025	0.045
Stagnation temperature, u_{T_0}	0.020	0.03
Stagnation pressure, u_{p_0}	0.008	0.02
Mole fraction of water vapor, u_{x_v}	2.89	0
Reproducibility, u_{reprd}	0.035	< 0.01
Std. Combined Uncertainty Eq. (9), u_{C_d}	**0.05**	**0.05**
Expanded Uncertainty $U_{C_d} = k u_{C_d}$	[%, k = 2] **0.10**	[%, k = 2] **0.10**

5.4. Comparison Results and Discussion

For this bilateral comparison, the different operating pressures between NIST's and NIM's *PVTt* systems prevented the NMIs from calibrating the respective CFVs over a common Reynolds number range. Instead, the calibration results of the two NMIs are compared by linearly extrapolating NIST's C_d data to lower Reynolds numbers. The extrapolation is done in the laminar flow regime where C_d depends linearly on $Re_d^{-1/2}$. The applicability of this extrapolation has been demonstrated in other comparisons that used CFVs as transfer standards [6]. We expect the extrapolation to work well provided the boundary layer remains laminar. Generally speaking, laminar flow occurs for $Re_d < 10^6$, provided the CFV wall is smooth and there are no geometric defects upstream of the CFV throat section. Herein, the extrapolation

worked well for the 20 mm CFV, but had trouble with the 10 mm CFV attributed to the geometric defect observed in Fig. 3. Nevertheless, the extrapolation method was applied to both CFVs.

Figure 6 shows the comparison results for the 20 mm CFV. The NIST C_d data (◆) shows transition to turbulent flow at a Reynolds number of 10^6 (*i.e.*, $Re_d^{-1/2} = 0.001$). At Reynolds numbers below 10^6 (*i.e.*, $Re_d^{-1/2} > 0.001$), the NIST C_d data is laminar and follows a linear trend. The curve fit to the NIST data in the laminar regime has the functional form $C_d = 0.99864 - 3.191\,Re_d^{-1/2}$ and is depicted by the solid line (—) in Fig. 6. The standard deviation of the curve fit residuals is $d\,R_{FIT} = 0.0027$ % ($k = 1$). The dashed line (----) shows the extrapolation to the NIM data point (▲). The difference between the extrapolated NIST curve and the NIM data point is 0.11 %. The theoretical line (– · –) based on $C_{d,theory}$ in Eq. (6) agrees well both with NIST and NIM results, differing by at most 0.032 % from NIST and 0.05 % from NIM. All of the measured data had C_d values within the ± 0.3 % expanded uncertainty of the ISO 9300 curve fit (—) based on $C_{d,ISO}$ in Eq. (5).

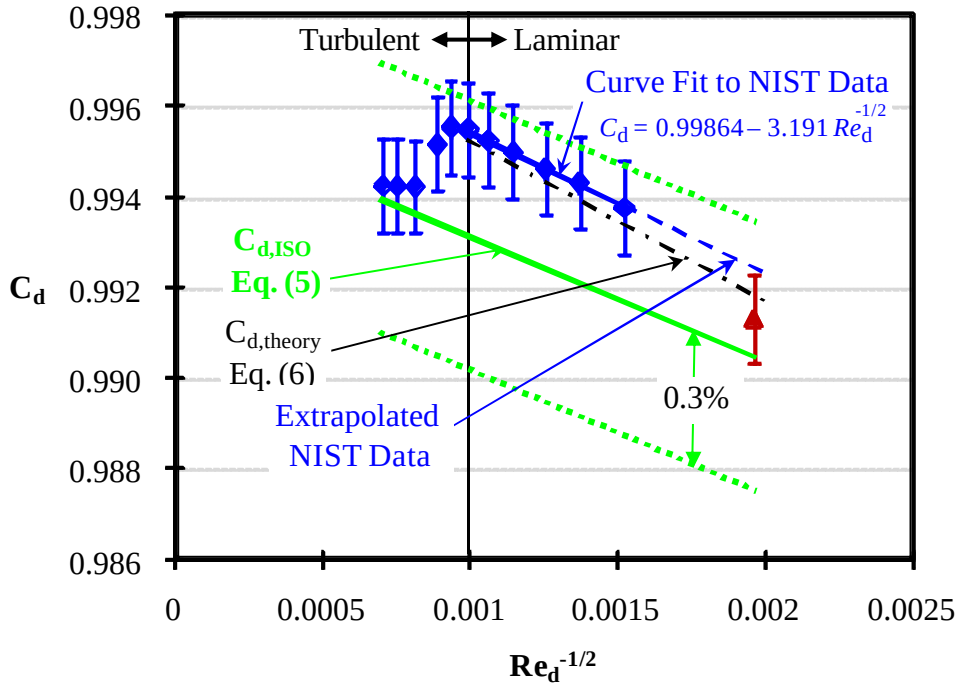

Fig. 6 The bilateral comparison results between NIM (▲) and NIST (◆) for d = 20 mm

Figure 7 shows the comparison results for the 10 mm CFV. The NIST C_d data (◆) shows no clear transition to fully turbulent flow. We suspect that the geometric defect near the throat of the 10 mm CFV (shown in Fig. 3) results in a local transition to turbulence at Reynolds numbers lower than expected. On the other hand, the boundary layer away from the defect is probably laminar until the Reynolds number reaches 10^6. Consequently, the C_d versus $Re_d^{-1/2}$ plot is not linear as expected. Nevertheless, the NIST data below Reynolds numbers of 6×10^5 (*i.e.*, $Re_d^{-1/2} > 0.00129$) is fit by the function $C_d = 1.00066 - 4.364\,Re_d^{-1/2}$, depicted by the solid line

(▬) in Fig. 7. The standard deviation of the curve fit residuals is $d\,R_{FIT} = 0.035$ % ($k = 1$). The dashed line (----) shows the extrapolation to the NIM data point (▲). The difference between the extrapolated NIST curve and the NIM data point is -0.017 %. Surprisingly, despite the geometric defect which is not accounted for in the theoretical model (– · –) based on $C_{d,theory}$ in Eq. (6) is in good agreement with the measured data. The maximum deviation of the NIST data is 0.067 % and the maximum deviation of the NIM data is 0.069 %. Similar to the 20 mm CFV, all of the measured values of C_d are within the ± 0.3 % expanded uncertainty limits of the ISO 9300 calibration curve (▬) based on $C_{d,ISO}$ in Eq. (6).

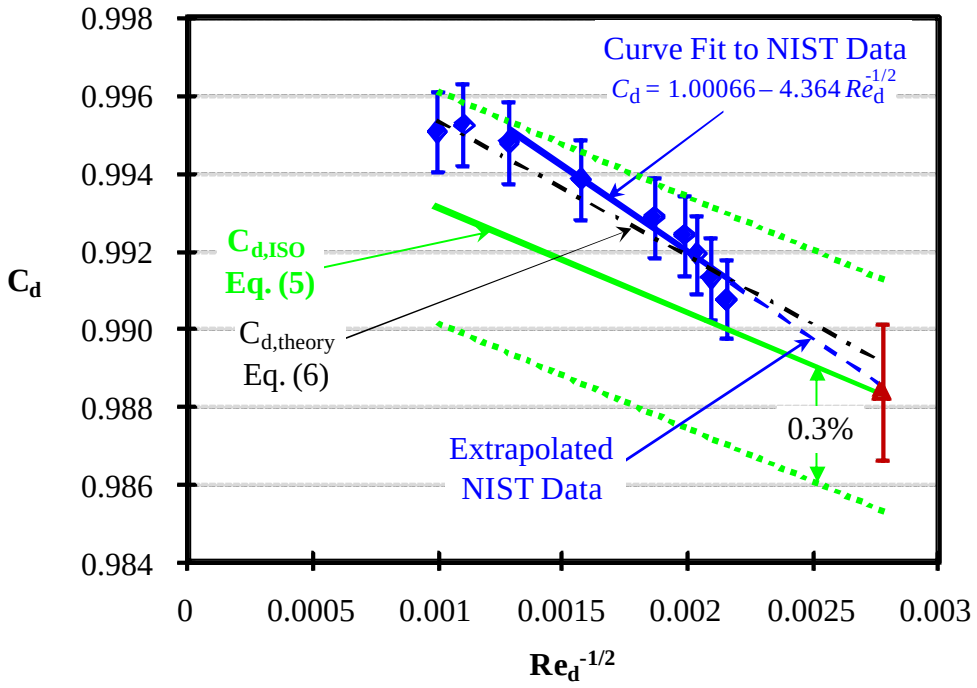

Fig. 7 The bilateral comparison results between NIM (▲) and NIST (◆) for d = 10 mm

The degree of equivalence between NIST and NIM is calculated by

$$E_n = \frac{100\left|\frac{C_{d,NIM}}{C_{d,NIST}} - 1\right|}{\sqrt{\left(\frac{C_{d,NIM}}{C_{d,NIST}}\right)^2 U^2_{C_{d,NIM}} + U^2_{C_{d,NIST}} + (2 \cdot d R_{FIT})^2}} \qquad (10)$$

where the numerator is the percent difference between the NIM and NIST values, and the denominator is the total expanded uncertainty, including a contribution from the fit residuals of the extrapolated curve fit. The degree of equivalence is demonstrated to be less than unity for both CFVs in Table 8.

Table 8. Summary of the Bilateral Results between NIM and NIST

Nom. Throat Dia. d_{nom}	NIM $C_{\mathrm{d,NIM}}$	Extrap. NIST $C_{\mathrm{d,NIST}}$	NIM vs. Extrap. NIST $100\left\lvert\frac{C_{\mathrm{d,NIM}}}{C_{\mathrm{d,NIST}}}-1\right\rvert$	NIM Expanded Unc. $U_{C_{\mathrm{d,NIM}}}$	NIST Expanded Unc. $U_{C_{\mathrm{d,NIST}}}$	Curve Fit Residuals $2\cdot dR_{\mathrm{FIT}}$	Degree of Equiv. E_{n}
[mm]	[ ]	[ ]	[%]	[%, k = 2]	[%, k = 2]	[%, k = 2]	[ ]
10	0.98838	0.98855	-0.017	0.18	0.10	0.069	0.08
20	0.99132	0.99238	-0.107	0.10	0.10	0.0054	0.74

6. Conclusions

The bilateral comparison between NIM and NIST was conducted from June 2008 to October 2009. Two CFVs with nominal throat diameters of 10 mm and 20 mm were selected as transfer standards. The CFVs were calibrated in air with NIM's 20 m^3 *PVTt* at atmospheric conditions, and subsequently with NIST's 26 m^3 *PVTt* at stagnation pressures ranging from 170 kPa to 800 kPa. The resulting data was compared by extrapolating the NIST data in the laminar regime to the lower NIM flow. The NIST discharge coefficients were extrapolated using a linear function of $Re_{\mathrm{d}}^{-1/2}$ in accordance with CFV flow theory. The NIST data followed the expected linear trend for the 20 mm CFV and consequently the extrapolation method worked well. In contrast, the NIST data for the 10 mm CFV was not a linear function of $Re_{\mathrm{d}}^{-1/2}$, possibly due to a geometric defect just upstream of its throat section. We suspect that the defect caused a low Reynolds number transition to turbulent flow near the defect, but away from the defect the flow remained laminar up to the typical transition Reynolds number of 10^6. The parallel laminar and turbulent flows could generate the non-linear calibration curve measured by NIST. Nevertheless, the extrapolation method was implemented for both CFVs, although the defect introduced substantially more uncertainty in the case of the 10 mm CFV. The comparison results for both CFVs were in good agreement as demonstrated by the degree of equivalence being less than unity ($E_{\mathrm{n}} < 1$). Furthermore, the experimental results for both CFVs agreed well (*i.e.*, better than 0.07 %) with existing theoretical models, which added confidence to the extrapolation method. The ISO 9300 empirical equation showed systematic differences with measured data, but was within its ± 0.3 % expanded uncertainty limits.

References

[1] Wright, J. D., *The Long Term Calibration Stability Of Critical Flow Nozzles And Laminar Flowmeters*, Proceedings of the 1998 NCSL Workshop and Symposium, Albuquerque, NM: NCSL, pp. 443-462, 1998.

[2] Johnson, A. N., and Wright, J. D., *Revised Uncertainty Analysis of NIST 26 m^3 pVTt Flow Standard"*, P Proc. of the International Symposium on Fluid Flow Measurement, Queretaro Mexico, 2006.

[3] Johnson, A., and Wright, J., *Comparison between theoretical CFV flow models and NIST's primary flow data in the laminar, turbulent and transition flow region*, Journal of Fluids Engineering. 2006, 130 (071202) , pp. 1-11, 2008.

[4] Ishibashi, M., *Proposal of Fluid Dynamical Standard (FDS) for Gas Flow-Rate*, Proc. of the International Symposium on Fluid Flow Measurement, Arlington, USA, pp. 7-10, 2002.

[5] Ishibashi, M., Takamoto, M., *Theoretical discharge coefficient of a critical circular-arc nozzle with laminar boundary layer and its verification by measurements using super-accurate nozzles*, Flow Measurement and Instrumentation, 11, pp. 305-311, 2000.

[6] Mickan, B., Kramer, R., Dopheide, D., Hotze, H.-J., Hinze, H.-M., Johnson, A. N., Wright, J. D., and Vallet, J.-P., *Comparisons by PTB, NIST, and LNE-LADG in Air and Natural Gas with Critical Venturi Nozzles Agree within 0.05 %*, Proc. of the International Symposium on Fluid Flow Measurement, Queretaro, Mexico, 2006.

[7] ISO 9300, Measurement of Gas Flow by Means of Critical Flow Venturi Nozzles, 2005.

[8] Johnson, A. N., and Wright, J. D., *Evaluation of Theoretical CFV Flow Models in the Laminar, Turbulent, and Transition Flow Regimes*, Proc. of the International Symposium on Fluid Flow Measurement, Queretaro, Mexico, 2006.

[9] J R Kliegel and J N Levine. *Transonic flow in small throat curvature radius nozzle*s, AIAA, 7: 1375-1378, 1969.

[10] Geropp, D., *Laminare grenzschichten in ebenen und rotationssymme-trischen lavalduesen.* Deutsche Luft-Und Raumfart, pp. 71-90, 1971.

[11] Stratford, B. S., *The calculation of the discharge coefficient of profiled choked nozzles and optimum profile for absolute airflow measurement*, The Royal Aeronautic Society, 68:237-245, 1964.

[12] Johnson, A. N., and Wright, J. D., *Gas Flowmeter Calibrations with the 26 m^3 PVTt Standard*, NIST Special Publication 1046, 2005.

[13] ISO/IEC Guide 98, *The Guide to the Expression of Uncertainty in Measurement (GUM)*, 1995.

[14] Aschenbrenner, A., *The Influence of Humidity on the Flowrate of Air through Critical Flow Nozzles*, Flomeko, 1983.

[15] Britton., C, L., Carron, R. W., and Kegel, T., *The Critical Flow Function, C*, for Humid Air*, 1998 ASME Fluids Engineering Division Summer Meeting FEDSM98-5309, 1998.